Hittite Journal of Science and Engineering, 2020, 7 (2) 115-123
ISSN NUMBER: 2148-4171
DOI: 10.17350/HJSE19030000180

2D and 3D Positioning Performance of UAV-Based Photogrammetry in Residential Regions

Mehmet Nurullah Alkan[1] Kayhan Aladogan[1] Zafer Kose[1] Oyku Alkan[2]
[1]Hitit University, Osmancık Vocational School, Corum, Turkey
[2]Istanbul Technical University, Graduate School of Science Engineering and Technology, Istanbul, Turkey

ABSTRACT

UAVs (Unmanned Aerial Vehicles) are commonly used in photogrammetric observations in research fields like agriculture, archaeology, industry and construction of base maps. They present several advantages like low-cost platforms, rapid results, high positioning accuracy and less labor effort in the field.

In this study, we evaluate the positioning accuracy of UAV based photogrammetry with conventional observation techniques in a sample area. Our main motivation is to examine if the final model of a low altitude UAV can reach the positioning accuracy of conventional observation techniques, especially in residential regions. For this purpose, we evaluate the results of 3 separate photogrammetric flights in a pre-observed field. Results indicate that low-altitude UAV flights can provide high accuracy both in 2D and 3D positioning in residential and densely constructed areas.

Keywords:
UAV, Photogrammetry, GNSS, Terrestrial observations, SfM, Positioning accuracy.

Article History:
Received: 2020/02/17
Accepted: 2020/06/03
Online: 2020/06/26

***Correspondence to**: Mehmet Nurullah Alkan, Hitit University, Osmancik Vocational High School*
E-mail: nurullahalkan@hitit.edu.tr,
Phone: +90 532 432 9145,
Fax: +90 364 611 5030.

INTRODUCTION

Photogrammetry has been widely used for acquiring field data, which has much more better spatial resolution than remote sensing. Also, close range aerial photogrammetry by using unmanned platforms is a new concept considering other techniques and methods. Using that technique is mainly based on the necessity for low-cost and less labor applications. Aim is to extract geo-referenced information of the interested objects and/or regions in a wide range of data diversity by automated processing with the help of stereo aerial imagery [1-7].

Considering the aim and purpose, model from a UAV flight can procure accurate data in a wide range of small to large scaled projects (Fig. 1) [1, 4]. In this concept, requirement and applications of UAV photogrammetry vary from agriculture to forestry, archeology, geology and even specific activities like measurement of the tree heights for monitoring the development of the forestland, soil displacement and such civil engineering applications [1-6, 8].

Nowadays, there are several types of those UAV platforms (fixed or rotary wings, etc.) with mounted digital sensors for different purposes that allow to model ground truth by using multiple scene data in a short-time window. Also, UAVs for photogrammetric applications generally include a GNSS (Global Navigation Satellite System) sensor combined with an INS (Inertial Navigation System) unit for automatic take-off and landing, acquiring images, calculating precise position of the imagery sensor and certain parameters at the time of the photo-shoot. Those information are inputs for constitution of an accurate photogrammetric model of the scenery. UAV platforms generally have a mounted digital camera to acquire photos but in some cases, that camera type can be rearranged to have a LIDAR (Light Detection and Ranging) or multispectral image sensors according to the pre-determined conditions of the study [1, 3, 6, 9].

A UAV-based photogrammetric model is based on some certain steps like a flight trajectory plan, observation of common points (on the ground and images), creating a point cloud and constitution of 3D models, respectively. As a result, final outputs of a UAV flight can be used for creating ortho-images, digital terrain models, gathering metric information and even 3D mo-

del of the area. Another benefit of UAV platforms is that they can adopt to certain changes on the field because of their quick response time and model constitution [1, 3, 6, 10].

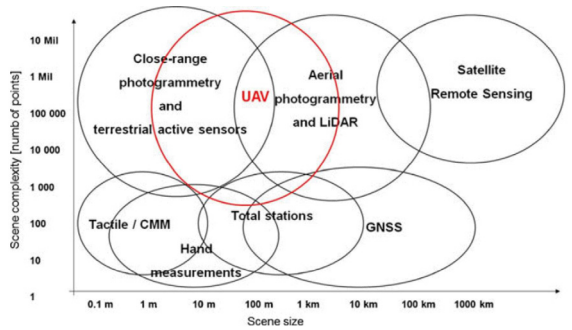

Figure 1. Available techniques and sensors for data acquisition and UAV based photogrammetric model in the manner of number of points in the point cloud and magnitude of the project area (from [1]).

METHODOLOGY FOR A UAV-BASED PHOTOGRAMMETRIC MODEL

Important variables should be considered before a UAV flight. Those are important parameters and may vary from scene to scene and should be adopted according to the analysis of the study area (Fig. 2):

- Aim of the project (emergency situation or precise model constitution),
- Required ground sampling distance (GSD) based on the subject,
- Size of the area,
- Flight trajectory and energy consumption of the platform,
- Overlap ratios for the photos [1, 5, 7-8, 11-13],
- Data process time.

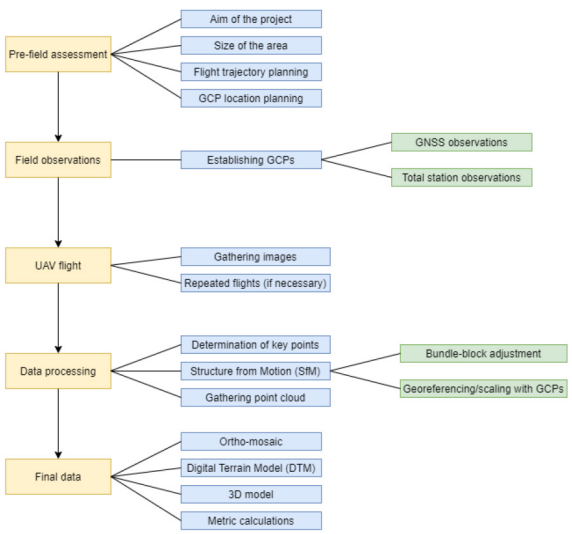

Figure 2. Workflow of a UAV based photogrammetry [2, 5, 14].

Those UAV-based photogrammetric models requires a pre-field study if the scenery information is essential with the ground coordinate system. That process is generally realized by using common points (Ground Control Points - GCPs) both available on the images and on the ground. A GCP is a pre- or post-observed point used for image transformation between image-ground coordinate systems, which can be defined as manual key points. Their coordinates can be estimated before or after the flight and can be chosen as distinct objects or can be manually established on the ground by the user [15]. General approach to acquire the position of the GCPs are related with RTK (Real-time kinematic) or network-based GNSS observations nowadays to increase the accuracy of the model. Later on the process, multiple GCPs are used for geo-referencing and scaling the mosaic overview of the interested area. But a more recent advance is to use a UAV with combined RTK-GNSS and INS modules which allows to estimate the coordinates of the photo-shoot point and orientation parameters on board [1, 5, 7, 10, 11, 16].

In general, main issue to acquire data from scene photos is to establish a correlation between the photo-plane and the ground truth and that can be realized by using GCP data. In the constitution of the final 3D model, all photos from the imagery sensor evaluated together by using bundle-block adjustment, which can eliminate systematic errors with the help of a minimum number of GCPs on the scene. That step includes a coordinate transformation and there should be at least 3 known points at both images and the ground to gather information later from the photos. The number of GCPs can be increased if the elevation of the region has abrupt changes [1, 4, 5, 11, 17].

For traditional photogrammetry, the link between those coordinate systems requires parameters such as interior orientation values for the camera (calibration report) and

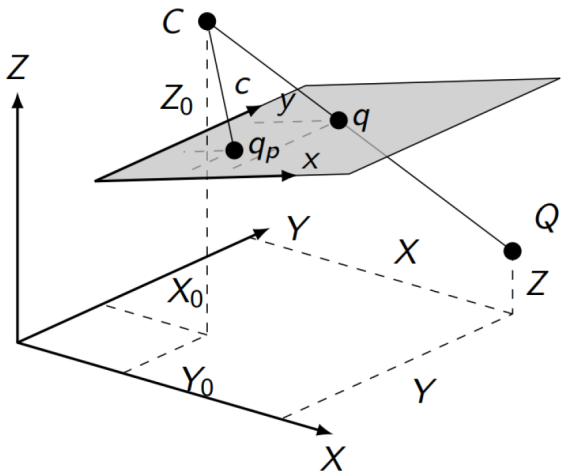

Figure 3. Relationship between a ground point (Q), camera center (C) and the orientation of the photo plane regarding the terrestrial coordinate system [18].

certain features (GCPs) both visible and observable on the image and on the ground for the exterior orientation variables [1, 5, 11] (Fig. 3).

It can be derived from Fig. 3 that XYZ axes are the ground coordinate system and xy axes are photo plane system. Also, c represents the principal distance, q_p is the principal point and X_0, Y_0, Z_0 are the coordinates of the camera center in terrestrial coordinate system [18]. Regarding the position of the camera and its orientation, the collinearity equation can be written as follows:

$$x - x_p = -c\frac{r_{11}(X - X_0) + r_{21}(Y - Y_0) + r_{31}(Z - Z_0)}{r_{13}(X - X_0) + r_{23}(Y - Y_0) + r_{33}(Z - Z_0)} \quad (1)$$

$$y - y_p = -c\frac{r_{12}(X - X_0) + r_{22}(Y - Y_0) + r_{32}(Z - Z_0)}{r_{13}(X - X_0) + r_{23}(Y - Y_0) + r_{33}(Z - Z_0)} \quad (2)$$

In the equation:

- x, y : Coordinates of the image point (q)
- X, Y, Z : Coordinates of the ground point (Q)
- x_p, y_p : Coordinates of the principal point
- X_0, Y_0, Z_0 : Coordinates of the camera center in terrestrial coordinate system
- $r_{11} - r_{33}$: Angular orientation matrix along 3 axes between photo-ground coordinate system [11, 19].

However, with a bundle-block adjustment approach, all required parameters can be computed automatically with high precision. That procedure is known as "Structure from Motion (SfM)", an automated model constitution from images, and such software solutions can combine SfM with bundle-block effectively. That allows using multiple imagery from different platforms and does not require specific camera orientation parameters or precise position [1, 11, 5, 14, 8, 20].

The next step, image assessment, involves the analysis of every image from the scene and estimating the common features or points to link and chain all data. That is established by calculating the camera positions and orientation parameters for each image simultaneously which is derived from SfM approach. Point cloud data in that stage does not have a scale or orientation, but that procedure is completed by using a minimum number of GCP variables [5, 7-8].

The final output of a UAV-based photogrammetric model generally includes an ortho-mosaic view of the scene and a 3D model which may used for metric calculations such as distance, volume, base map construction, etc. Accuracy of the constructed photogrammetric model may vary, but is up to centimeter-decimeter level according to the scenery variables(flight altitude, camera specifications, etc.). Such regulations limit the position accuracy to a certain level, but necessary precision can be derived by a UAV model [1, 6-9, 14, 21].

MATERIAL AND METHODS

Model Area

In this study, the research area is located in the Osmancık campus of Hitit University in Çorum, which consists of a main building with two playfields, recreational areas and parks. Vegetation is sparse considering wood density and area is suitable for both geodetic observations and UAV flights, with no significant flight obstacles around. Campus area is about 0.05 km^2 in total and land elevation ranges between ~420 – 445 m. That gives a height difference roughly above 20 m and 5% slope at its maximum, thus the area can be defined as low-pitched (Fig. 4).

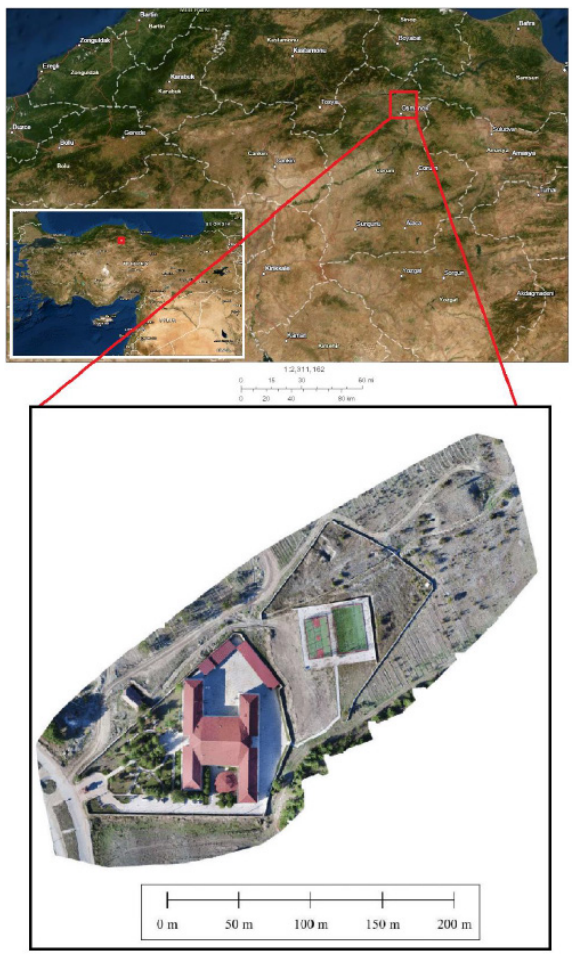

Figure 4. Location of the study area and Hitit University Osmancık campus general overview (after [22]).

We focused on the main structure at the center of the campus. That is a double-floored concrete building and has a height around 7 m, but it is not a classical 4-cornered building. It looks like a tilted "H" and has deep corners. We

Figure 5. Main building of the campus from the parking lot at the north side. Fringe(yellow) and one of the deep corners(blue) are marked on the figure.

established two different field observations to acquire the field data for the characteristic points of that structure. First one is the terrestrial observations (joint GNSS and angle-distance surveying) and the second one is based on 3 different photogrammetric model flights with different altitudes. After acquiring the coordinates of characteristic points with two different methods, we made an evaluation considering both results (Fig. 5).

Data Acquisition

Terrestrial Observations

There are 9 benchmarks established on the field and geodetic observations are based on those points (Fig. 6). Location data for all the corners of the main building is derived using GNSS and total station observations, respectively. Because, obstacles are covering the open sky view (mainly caused by the building and fringes) and make it almost impossible to estimate the coordinates of the structure by GNSS observations.

At first, we used a Spectra SP80 GNSS receiver for 2 sessions to calculate the average coordinates of the benchmarks in the area. After that, we conducted observations

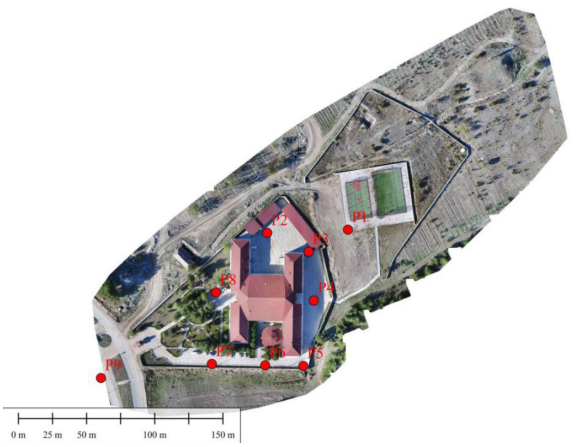

Figure 6. Location of the benchmarks used in data acquisition of the main structure in the campus with terrestrial observations.

Figure 7. Main structure at the center of the campus from above. 12 red dots are regular corners (C), and 8 white dots are deep corners (DC).

with a total station for final 3D coordinate acquisition of the building's characteristic points. The specifications of GNSS device and the observations are given at Table 1.

The locations of the benchmarks which are based on the network-RTK observations are given in Fig. 6. GNSS observations on those points completed by using TUSAGA-Aktif, a continuously operating GNSS network. It has 158 control points all around Turkey and allows the GNSS receivers to obtain real-time coordinates of any point on the terrain which has open sky view for satellite transmissions [24]. The positioning accuracy of the real-time GNSS observations are below ±3 cm in horizontally and ±5 cm vertically while using this network [25-26].

We concentrated our observations on the main building's corners and deep corners. Moreover, we acquired a total of 20 points' coordinates (Fig. 7). We used the benchmarks at appropriate locations around the structure with a Spectra Focus 8 total station. That device has a 2" angle and (2 mm ± 2 ppm) distance precision and suitable for data acquisition and the construction of base maps [27]. We used that device because it also has the capability to make observations using a laser beam without a reflector and allow direct targeting to the interested points (corners of the structure) which eliminates the offset error. Thus, data acquisition for interested points were mainly based on the combined angle and the distance measurements with that instrument.

Photogrammetric Data Acquisition

We used a DJI Phantom 4 Pro UAV for photogrammetric model construction, which has a 20 M resolution camera with 1" CMOS, the ability to take-off/land vertically and a Satellite Positioning System that works with both GPS (Global Positioning System) and GLONASS (Global Navigation Satellite System) [28].

Table 1. Specifications of the GNSS receiver and observation limitations [23]. Used GNSS satellites are marked with (*).

Receiver type	*Spectra SP80 Multi-frequency GNSS receiver (compatible with GPS*, GLONASS*, BeiDou, Galileo, QZSS, SBAS, IRNSS)*					
Precision in Network RTK	*8 mm ± 0.5 ppm horizontal*			*15 mm ± 0.5 ppm vertical*		
Satellite cut-off angle	*10°*					
Number of epochs for both sessions/point	*20*					
Epochs/second	*1*					
Gap between sessions	*>1 hour*					
Final coordinates	*Average coordinates of 2 sessions*					
Datum	*ITRF96*	*Mean meridian*	*36*		*Zone width*	*3°*
Ellipsoid	*GRS80*	*Reference epoch*		*2005.0*		
Observation mode	*Network RTK (VRS)*	*Connected network*		*TUSAGA-Aktif*		

We evaluated the field data with Pix4D software and it is advised that there should be well-distributed 5-10 GCPs in the working area by the manufacturer [5, 17]. Thus, before the flight, we established 6 temporary GCPs around the sampling area according to that initial information. The locations of GCPs are selected to have a normal distribution on the field as far as possible which might have a great influence on the accuracy of whole model [8, 14]. The coordinates of those points were acquired by using Spectra SP80 GNSS receiver with network-RTK method and their locations and ground materials are given at Figs. 8 and 9.

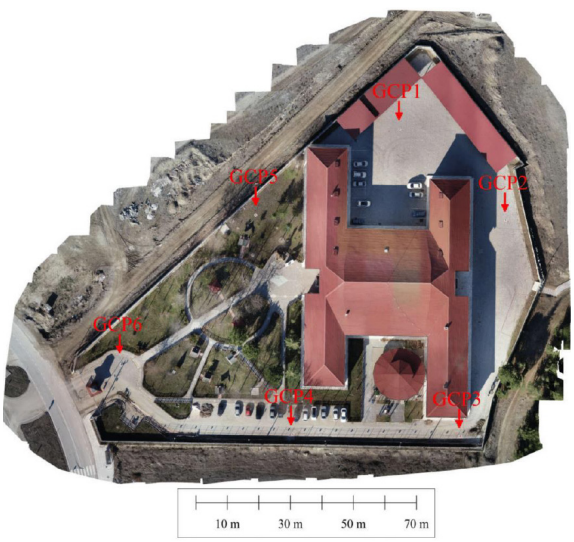

Figure 8. Location of the GCPs around the model area.

Figure 9. One of the temporary GCPs established on the ground for each flight. Image on the left is from actual photo of the feature and the right one is obtained from densified point cloud.

We conducted 3 different flights at different altitudes and selected different side and front overlaps for each trajectory (Table 2).

Table 2. Front and side overlap ratios for 3 different flight altitudes of the UAV.

Flight No	*Height*	*Front overlap*	*Side overlap*	*Number of photos*
1	*30 m*	*90%*	*70%*	*500*
2	*45 m*	*80%*	*70%*	*111*
3	*60 m*	*80%*	*70%*	*65*

1st flight's front overlap ratio differs from the other flights due to the improper photo-shoot point of the UAV at deep corners. There should be at least 2 photos for each corners to estimate actual coordinates, however, at 30 m height with lower front overlap (80%), that condition did not match due to the flight trajectory of the UAV. Thus, we increased the front overlap ratio to 90% for that altitude (Fig. 10).

A drawback with photogrammetric flight plan occurs that the main construction in the campus has deep corners which makes them hard to observe from all angles at the flying altitudes of the UAV. Additionally, the building has a low fringe height (~6 m). This is another drawback for data acquisition because they can completely or partially block the view of the flying platform due to improper photo-shoot point/flight plan, height or front/side overlap ratios of the UAV. Thus, we rearranged the flying trajectories and altitudes to eliminate those concerns.

We evaluated the final data with Pix4D software, which uses the photos from UAV and GCP data as input within several steps, based on aerial triangulation and bundle block adjustment [1, 29]. Results of the Pix4D process for each flight are given at the Table 3.

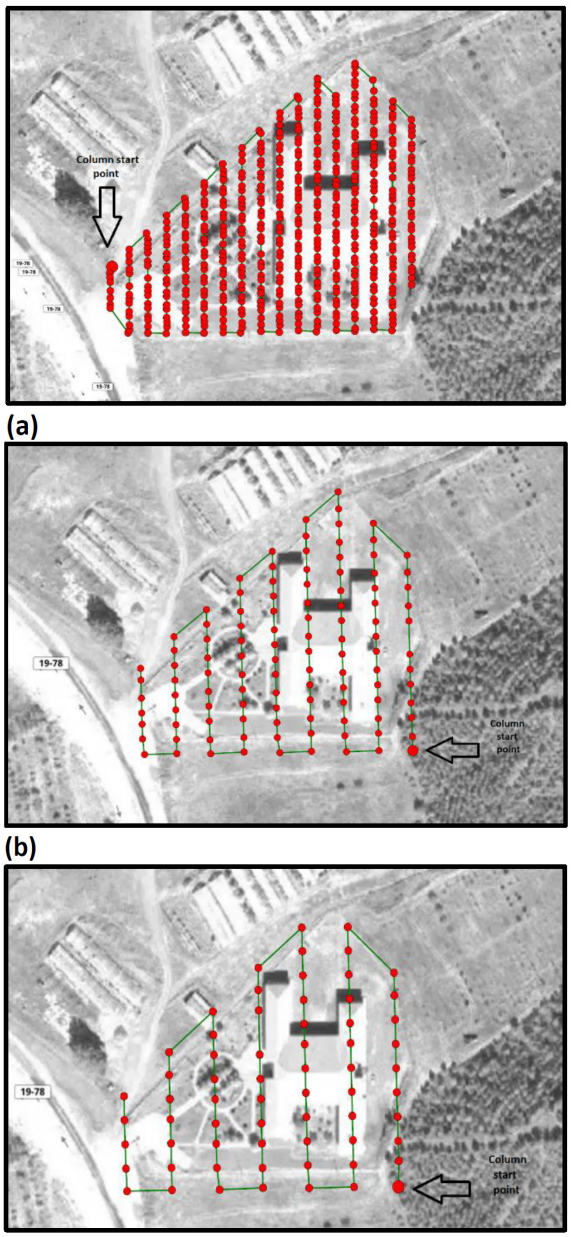

Figure 10. Flight plan for 3 different altitudes, (a) 30 m, (b) 45 m, and (c) 60 m, respectively. Red dots represents every photo-shoot point of the UAV during the flight and green lines indicates the trajectory of the platform.

Table 3. Pix4D processing results for 3 flight plans.

Flight No	*30 m flight*	*45 m flight*	*60 m flight*
Average Ground Sampling Distance (GSD)	*0.71 cm*	*1.12 cm*	*1.53 cm*
Model Area	*0.020 km²*	*0.027 km²*	*0.031 km²*
Number of images/ calibrated images	*500/500*	*111/111*	*65/65*
Error for GCPs georeferencing (mean RMS)	*0.011 m*	*0.012 m*	*0.012 m*
Mean reprojection error for Bundle Block Adjustment	*0.164 pixel*	*0.161 pixel*	*0.16 pixel*

After the full process of each flight, the characteristic points of the main structure were digitized using Pix4D interface and coordinates were acquired for further evaluation. There is a total of 20 points from the terrestrial observations and they were all matched with the Pix4D digitizing process.

At this phase, the corners are more visible in the photos (5-31 photos) then the deep corners (2-8 photos) as expected (Table 4&5), but visibility highly depends on the environmental conditions. In order to produce coordinate data from the photogrammetric model, all corners should be observed from at least 2 photos. Considering the flights, all corners are visible and match that condition. However, from three different models, we evaluated that fringes, improper photo-shoot position of the UAV, vegetation, sun light reflection on the white edges and even shadows prevent a clear view and digitizing of the characteristic points of the structure (Figs. 11 and 12). But those obstacles were obviated by using multiple photos of the interested points.

Table 4. Characteristic points of the building and their visible number of photos from different altitude UAV flights (C: corner, DC: deep corner).

Point No	*Visible in number of photos*		
	30 m flight	*45 m flight*	*60 m flight*
C1	*17*	*5*	*5*
C2	*31*	*11*	*11*
C3	*25*	*13*	*12*
C4	*24*	*9*	*8*
C5	*24*	*8*	*7*
C6	*24*	*8*	*7*
C7	*8*	*8*	*6*
C8	*15*	*9*	*10*
C9	*31*	*12*	*14*
C10	*16*	*7*	*7*
C11	*20*	*9*	*8*
C12	*22*	*9*	*10*
DC1	*6*	*4*	*4*
DC2	*6*	*4*	*4*
DC3	*6*	*4*	*2*
DC4	*7*	*3*	*2*
DC5	*6*	*2*	*3*
DC6	*4*	*4*	*2*
DC7	*8*	*4*	*4*
DC8	*6*	*6*	*5*

Table 5. Average number of photos for each flight.

	30 m flight	*45 m flight*	*60 m flight*
Average number of photos for corners (C)	*21.4*	*9.0*	*8.8*
Average number of photos for deep corners (DC)	*6.1*	*3.9*	*3.3*
Number of photos for DC/C	*0.29*	*0.43*	*0.37*
Overall number of photos for DC/C		*0.36*	

Figure 11. Challenges acquiring data from photogrammetric model. Shadow of the manmade structures and/or vegetation may prevent a proper positioning. At DC5, shadow of vegetation around the corner partially block the view and makes it harder to assess the actual location. Green cross represents the estimated location and yellow circle is the error estimation for the point.

Figure 12. Challenges acquiring data from photogrammetric model. At C12, color of the building over-radiated at the time of photoshoot and may lead to a poor positioning assessment. Green cross represents the estimated location and yellow circle is the error estimation for the point.

The coordinates of the characteristic points of the interested structure were all estimated by before mentioned methods. Thus, we finally had 1 set of data from terrestrial observations and 3 sets of data from 3 different photogrammetric models for further evaluation.

RESULTS AND DISCUSSION

We interpreted final data in the manner of location accuracy and evaluated every photogrammetric model results separately with terrestrial observations in 2D and 3D (Table 6 and 7).

Results indicate that the position differences ranges between 0.005 – 0.138 m in 2D and 0.02 – 0.181 m in 3D, considering all flights. In addition, the maximum positioning error at 60 m altitude is greater than other flights in 2D and 3D positioning and those differences occur especially at deep corners. At points DC1, DC3, DC4, DC5 and DC6 for 60 m flight, 2D and 3D positioning errors are roughly above a decimeter. Considering Table 4, those corners are visible only from 2 – 4 aerial photos, thus that might lead to estimate the position of the point poorly [5]. We evaluated that those certain errors may arise from certain features such as higher flight altitude and/or lower resolution due to that trajectory. However, considering overall performance of all photogrammetric models, there is no significant difference

Table 6. Cross-validation of coordinate differences at each point between terrestrial observations and photogrammetric model results (C: corner, DC: deep corners).

	30 m		45 m		60 m	
Point No	2D pos. dif.(m)	3D pos. dif.(m)	2D pos. dif.(m)	3D pos. dif.(m)	2D pos. dif.(m)	3D pos. dif.(m)
C1	0.068	0.073	0.056	0.060	0.090	0.090
C2	0.030	0.034	0.037	0.037	0.011	0.016
C3	0.035	0.068	0.027	0.028	0.020	0.020
C4	0.035	0.045	0.026	0.032	0.009	0.017
C5	0.057	0.058	0.058	0.068	0.091	0.091
C6	0.037	0.068	0.023	0.067	0.024	0.031
C7	0.018	0.045	0.009	0.054	0.013	0.052
C8	0.014	0.036	0.014	0.034	0.029	0.068
C9	0.020	0.038	0.021	0.024	0.024	0.066
C10	0.046	0.082	0.049	0.052	0.037	0.068
C11	0.050	0.056	0.059	0.068	0.042	0.060
C12	0.024	0.060	0.024	0.025	0.041	0.062
DC1	0.009	0.020	0.005	0.036	0.069	0.111
DC2	0.029	0.057	0.042	0.048	0.020	0.026
DC3	0.085	0.092	0.054	0.074	0.138	0.181
DC4	0.057	0.088	0.036	0.076	0.080	0.120
DC5	0.045	0.094	0.027	0.090	0.115	0.131
DC6	0.061	0.093	0.052	0.056	0.093	0.111
DC7	0.014	0.085	0.027	0.043	0.025	0.043
DC8	0.042	0.048	0.029	0.040	0.008	0.017

Table 7. Statistics for each flight considering terrestrial observations.

	30 m model		45 m model		60 m model	
	2D	3D	2D	3D	2D	3D
Min. (m)	0.009	0.02	0.005	0.024	0.008	0.016
Max. (m)	0.085	0.094	0.059	0.09	0.138	0.181
Mean (m)	0.039	0.061	0.034	0.051	0.049	0.069
RMS. (m)	0.045	0.066	0.038	0.055	0.064	0.084

in mean error in 2D (0.039 – 0.049 m) and in 3D (0.051 – 0.069 m) and in the manner of RMS in 2D (0.038 – 0.064 m) and in 3D (0.055 – 0.084 m).

RMS values for each flight at Table 7 indicates the standard deviation of the residuals for the positioning of each point. That might give us an overlook for the results in general.

Values are below 0.07 m in 2D and 0.09 m in 3D positioning for all flights. These can be considered as statistically valid if the positioning errors are in a predefined limit. For that reason, there should be some limitations and regulations to eliminate the error sources and take the results to a certain confidence level. Considering the construction of base maps, in specific, Turkey has strict rules for that purpose [21]. After completing a photogrammetric model, values derived from it, can be controlled in such ways to find out the consistency of the observations. General process for that

purpose is established by comparing the photogrammetric results with terrestrial observations (GNSS, etc.). Actually, we have conducted that condition in our study.

While controlling our model accuracy, we used Table 6 as an outcome. According to the regulations in Turkey, coordinates of a certain percentage of detail points in a base map, derived by photogrammetry, should be controlled or compared by GNSS or total station observations. That process includes 2D position and height differences separately and leads the photogrammetric model to offer certain errors below those limits:

$$RMS_{X,Y} < \pm\left(-1{,}665\times10^{-6}\times S^2 + 0{,}01745\times S - 1{,}166\right) \quad (3)$$

$$RMS_Z < \pm RMS_{X,Y}\times 1{,}33 \quad (4)$$

where S is the denominator of the scale of the base map [21]. Considering the equations above, RMS values can be calculated for a 1/500 scale base map as ±0.071 m and ±0.095 m, respectively. From Table 7, derived RMS values for each flight are below those calculated limitation values in both 2D and 3D positioning. Our photogrammetric models have positioning errors, but according to the results, they can supply adequate accuracy comparable with terrestrial observations. And considering the RMS values derived in this study, a photogrammetric survey model can offer high accuracy during the construction of base maps; not in only rural areas, but also in highly populated/constructed zones.

On the other hand, there is no clear evidence for an improvement in positioning when we lowered the flight altitude from 45 m to 30 m. Additionally, 45 m flight gives better performance than 30 m in this study for mean error (0.051 m/0.061 m) and RMS (0.055 m/0.066 m) values at their maximum. That might indicate that lowering the flight altitude may not contribute a significant difference in photogrammetric modeling in every situation.

In this study, we evaluated 500, 111, and 65 photos for 30 m, 45 m and 60 m flights, respectively. That is an important issue while planning the photogrammetric model because there should be much more photos with lowering the flight altitude. That concludes a significant increase in both flight and software processing time and might be an important issue if the final data is crucial in a short time window.

Main issue in this study was to estimate the proper locations of the deep corners. They are visible from a minimum number of photos considering regular corners and data acquisition might lack of accuracy at those points. During our UAV flights, we evaluated that the deep corners can only be observed with less then ~36% view angle from the sky (Table 5). Thus, for gathering full view of every structure corners, we recommend increasing the side and front overlap ratios during the flight or widening the model area with longer flight trajectory. By that way, UAV can have more photo-shoot points while advancing through the edges of the flight trajectory. Although our study area is not in a highly populated region, one might notice that this condition might emerge in every residential territory which has squeezed constructed regions.

During this study, we planned the altitude of the UAV almost 4, 6 and 8 times of the interested building height (~7 m). Heights of the structures might differ at different regions, but if there are certain features which has deep corners like our study, we recommend the flight altitude to not exceed ~45 m for a UAV flight on the field, if the specifications of the device is similar to ours [28].

In addition, positioning accuracy might depend strongly in some conditions, such as over radiated corners due to sunlight or view block by vegetation or their shadows. Our study conducted under those circumstances and we recommend to choose flight time-window during shorter shadows and lower vegetation if possible.

In conclusion, all the results indicate that UAV photogrammetry can provide high positioning accuracy as far as terrestrial observations. That condition might occur even in a highly populated and/or constructed regions while producing base maps and can reach to a centimeter and roughly decimeter level accuracy in 2D and 3D data acquisition.

References

1. Nex F, Remondino F. UAV for 3D mapping applications: a review. Applied Geomatics 6 (2014) 1–15.
2. Krause S, Sanders TGM, Mund JP, Greve K. UAV-based photogrammetric tree height measurement for intensive forest monitoring. Remote Sensing 11 (2019) 758.
3. Akturk E, Altunel AO. Accuracy assessment of a low-cost UAV derived digital elevation model (DEM) in a highly broken and vegetated terrain. Measurement 136 (2018) 382–386.
4. Barba S, Barbarella M, Benedetto AD, Fiani M, Limongiello M. Quality assessment of UAV photogrammetric archaeological survey. International Archives of the Photogrammetry, Remote Sensing and Spatial Information Sciences XLII(2)/W9 (2019) 93–100.
5. Bemis SP, Mickletwaite S, Turner D, James MR, Akciz S, Thiele ST, Bangash HA. Ground-based and UAV-based photogrammetry: a multi-scale, high resolution mapping tool for structural geometry and paleoseismology. Journal of Structural Geology 69 (2014) 163–178.
6. Uysal M, Toprak AS, Polat N. DEM generation with UAV photogrammetry and accuracy analysis in Sahitler Hill. Measurement 73 (2015) 539–543.
7. Fernandez T, Perez JL, Cardenal J, Gomez JM, Colomo C, Delgado J. Analysis of landslide evolution affecting olive

groves using UAV and photogrammetric techniques. Remote Sensing 8 (2016) 837.
8. Tomastík J, Mokros M, Salon S, Chudy F, Tunak D. Accuracy of photogrammetric UAV–based point clouds under conditions of partially–open forest canopy. Forests 8(5) (2017) 151.
9. Eisenbess H, Sauerbier M. Investigation of UAV systems and flight modes for photogrammetric applications. The Photogrammetric Record 26(136) (2011) 400–421.
10. Jiang S, Jiang W, Huang W, Yang L. UAV–based oblique photogrammetry for outdoor data acquisition and offsite visual inspection of transmission line. Remote Sensing 9 (2017) 278.
11. Dominici D, Alicandro M, Massimi V. UAV photogrammetry in the post–earthquake scenario: case studies in L'Aquila. Geomatics, Natural Hazards and Risks 8(1) (2017) 87–103.
12. Franco CD, Buttazzo G. Coverage path planning for UAVs photogrammetry with energy and resolution constraints. Journal of Intelligent & Robotic Systems 83 (2016) 445–462.
13. Cabreira TM, Franco CD, Ferreira Jr PR, Buttazzo GC. Energy–aware spiral coverage path planning for UAV photogrammetric applications. IEEE Robotics and Automation Letters 3(4) (2018) 3662–3668.
14. Martinez–Carricondo P, Agüera–Vega F, Carvajal–Ramirez F, Mesas–Carrascosa FJ, Garcia–Ferrer A, Perez–Porras FJ. Assessment of UAV–photogrammetric mapping accuracy based on variation of ground control points. International Journal of Applied Earth Observation and Geoinformation 72 (2018) 1–10.
15. Gonçalves JA, Henriques R. UAV photogrammetry for topographic monitoring of coastal areas. ISPRS Journal of Photogrammetry and Remote Sensing 104 (2015) 101–111.
16. Chudley TR, Christoffersen P, Doyle SH, Abellan A, Snooke N. High–accuracy UAV photogrammetry of ice sheet dynamics with no ground control. The Cryosphere 13 (2019) 955–968.
17. https://www.pix4d.com/blog/GCP–accuracy–drone–maps (last visited: 10.02.2020).
18. https://www8.cs.umu.se/kurser/5DV115/VT14/handouts/fundamentals_of_photogrammetry.pdf (last visited: 10.02.2020).
19. Zhang C, Yao W. The comparisons of 3D analysis between photogrammetry and computer vision. Paper Presented at XXIst ISPRS Congress Technical Commission III, Beijing, 3–11 July, pp. 33–36, 2008.
20. https://support.pix4d.com/hc/en–us/articles/205327965–Menu–Process–Processing–Options–1–Initial–Processing–Calibration (last visited: 10.02.2020).
21. https://www.hkmo.org.tr/resimler/ekler/466222ca92eaecb_ek.pdf (last visited: 10.02.2020).
22. www.arcgis.com (last visited: 10.02.2020).
23. http://trl.trimble.com/docushare/dsweb/Get/Document–844535/SG–SP80–Br–v2.pdf (last visited:10.02.2020).
24. https://www.tusaga–aktif.gov.tr/Sayfalar/IstasyonKonumBilgileri.aspx (last visited: 10.02.2020).
25. Aykut NO, Gülal E, Akpinar B. Performance of single base RTK GNSS method versus network RTK. Earth Sciences Research Journal 19(2) (2015) 135–139.
26. https://www.tkgm.gov.tr/sites/default/files/icerik/ekleri/tusaga–aktif_2018.pdf (last visited: 10.02.2020).
27. Spectra Precision Focus 8 total station user manual
28. https://www.dji.com/phantom–4–pro (last visited: 10.02.2020).
29. https://support.pix4d.com/hc/en–us/articles/205327965–Menu–Process–Processing–Options–1–Initial–Processing–Calibration (last visited: 10.02.2020).